



NIH PUBLIC ACCESS

Author Manuscript

J Mol Biol. Author manuscript; available in PMC 2008 November 17.

Published in final edited form as:

J Mol Biol. 2007 March 23; 367(2): 303–309. doi:10.1016/j.jmb.2006.10.017.

Structural Insights into Fibronectin Type III Domain Mediated Signaling

Sompop Bencharit^{1,2}, Cai Bin Cui³, Adnan Siddiqui³, Escher L. Howard-Williams⁴, John Sondek^{2,5}, Kheir Zuobi-Hasona⁶, and Ikramuddin Aukhil^{3,6,*}

¹ Department of Prosthodontics, School of Dentistry, University of North Carolina, Chapel Hill, NC 27599

² Department of Pharmacology, School of Medicine, University of North Carolina, Chapel Hill, NC 27599

³ Department of Periodontology, School of Dentistry, University of North Carolina, Chapel Hill, NC 27599

⁴ Department of Medicine, School of Medicine, Chapel Hill, NC 27599

⁵ Department of Biochemistry and Biophysics, School of Medicine, University of North Carolina, Chapel Hill, NC 27599

⁶ Department of Periodontology, College of Dentistry, University of Florida, Gainesville, FL 32610

Abstract

The alternatively spliced type-III extradomain B (EIIIB) of Fibronectin (FN) is only expressed during embryogenesis, wound healing and tumorigenesis. The biological function of this domain remains unclear. We describe here the first crystal structure of the interface between alternatively-spliced domain EIIIB and its adjacent FN type-III domain 8 (FN B-8). The opened CC' loop of EIIIB and the rotation and tilt of EIIIB domain allows good access to the FG loop of FN-8 which is normally hindered by the CC' loop of FN-7. In addition, the AGEQIP sequence of the CC' loop of EIIIB replaces the NGQQGN sequence of the CC' loop of FN-7. Finally, the CC'' loop of EIIIB forms an acidic groove with FN-8. These structural findings warrant future studies directed at identifying potential binding partners for FN B-8 interface, linking EIIIB to skeletal and cartilagenous development, wound healing, and tumorigenesis, respectively.

Keywords

fibronectin extradomain B; neovascularization; tissue regeneration

Introduction

Fibronectin (FN) is a multifunctional protein serving major roles in the adhesion, migration, differentiation and proliferation of cells with implications in embryonic development, wound healing, and tumorigenesis.¹ The significance of FN in embryonic development has been documented by the embryonic lethality seen in mice when the FN gene is disrupted.² FN is a high molecular weight dimeric glycoprotein with disulfide-linked subunits, each with a

*Address correspondence to: Ikramuddin Aukhil, P.O. Box 100434, Department of Periodontology, College of Dentistry, University of Florida at Gainesville, Gainesville, FL 32610, iaukhil@dental.ufl.edu.

Publisher's Disclaimer: This is a PDF file of an unedited manuscript that has been accepted for publication. As a service to our customers we are providing this early version of the manuscript. The manuscript will undergo copyediting, typesetting, and review of the resulting proof before it is published in its final citable form. Please note that during the production process errors may be discovered which could affect the content, and all legal disclaimers that apply to the journal pertain.

molecular weight of approximately 220–250 kDa. FN interacts with several other proteins in the ECM including collagen, heparin, fibrin, and cell membrane receptors. The amino acid composition of FN reveals it to be a large modular glycoprotein composed of homologous repeats of three prototypical types of domains known as types-I, II and III.³ Of these domains, FN type-III (FN-III) repeats are composed of \approx 90 amino acids making them the largest and most common of the FN subdomains.⁴ One of the best characterized interactions between FN and cell membrane receptors is the interaction between the RGD sequence of FN-III domain 10 (FN-10) and the extracellular domain of β 1-integrin.^{5–7} This interaction is believed to regulate integrin signaling and therefore may play an important role in integrin-mediated cell differentiation.^{8–10}

Among the type-III domains of FN that span the central part of FN molecule, three regions referred to as EIIIA, EIIIB and IIICS respectively, are subject to alternative splicing of a primary transcript.^{3–11} Of these spliced domains, EIIIA and EIIIB are either included or excluded by exon skipping and their alternative splicing is regulated in a tissue-specific and developmental stage-dependent manner.^{11–12} The amino acid sequence of alternatively spliced exons EIIIA and EIIIB is well conserved, suggesting their functional importance.¹³ Initial studies showed EIIIA and EIIIB splice variants of FN prominently expressed around developing blood vessels during embryonic development.^{14–15} These splice variants are absent in normal adult tissues except during wound healing and neoplastic vascularization. However, EIIIB- and EIIIA-null mice develop normally with only some small differences in wound healing, atherosclerosis and life-span in the EIIIA null mice.¹³ Fibroblasts cultured from EIIIB null mice grow slowly *in vitro* and deposit less FN in the pericellular matrix compared to fibroblasts cultured from wild-type mice.¹² EIIIB expression is predominantly found in breast and colorectal carcinomas. It was believed that tumor cells express EIIIB FN to recruit endothelial cells in order to supply the tumor mass with oxygen and nutrients. Thus, EIIIB may be one of a few clinical markers of neovascularization.¹⁶ Antibodies and variations of recombinant antibodies against EIIIB were proposed to be used in detections and treatments of several tumors including oral and mammary carcinomas.^{17–18}

The primary structure and electromicrographs suggested that FN-III is an extended molecule composed of repeated sequence motifs described as “beads on a string”.^{19–20} The crystal structure of FN type III domains 7 to 10 (FN7–10) that includes the RGD loop in domain 10 and the PHSRN synergy site in domain 9 has been previously published.⁴ The structure of FN-EIIIB alone was also solved by NMR.²¹ The individual FN type-III domains are very similar to each other and each domain consists of two β strands, one of four strands (G, F, C and C') and one of three strands (A, B, and E).⁴ Each domain in FN-III has low sequence identity (approximately 30% or lower), but they all have highly conserved secondary structural frameworks.^{4,21} The major variable factor between each FN-III domain is the interdomain interface which appears to be specific to each domain pair.⁴ Of interest, the interdomain buried surface area between type-III domains 7 to 10 varies and the maximum buried surface area is between domains 7 & 8.⁴ Similarly, the tilt between type-III domains 7–10 of FN also varies with the maximum tilt (52 degrees) between domains 7 & 8. There is unfortunately no general rule in the orientations between adjacent domains. EIIIB insertion between type-III domains 7 and 8 undoubtedly alters not only the interface, but possibly also the overall molecular polarity as a consequence of domain flips. As a consequence of the insertion of EIIIB between type-III domains 7 & 8, it was also hypothesized that these structural conformational changes of fibronectin would alter its interactions with other proteins thereby modulating extracellular signaling cascades in embryogenesis, wound healing, and neovascularization. To understand the role of EIIIB insertion and the interface between FN type-III domain extra domain B (EIIIB) and domain 8 (FN-8), we solved a 2.0 Å resolution crystal structure of FN-III fragment of EIIIB and FN-8. The structure reveals a unique interdomain relationship and provides structural insights into possible biological roles of EIIIB.

The Overall Structure of FN-B8

We initially attempted to crystallize the recombinant fragment of FN-III domain 7 (FN-7), EIIIB, and FN-8 (primary structure shown in Fig 1A). However, the crystals were too small and failed to yield sufficient x-ray diffraction. Since the FN 7–10 structure is already known⁴, we changed our strategy to make two shorter constructs-FN 7-B (FN-7 and EIIIB), and FN B-8 (EIIIB and FN-8). FN 7-B grew very small needle-like crystals that failed to yield sufficient x-ray diffraction. On the other hand, the FN B-8 fragment readily crystallized in 10–15% (w/v) PEG-3350 and 0.15–0.2 mM diammonium citrate((NH₄)₂HC₆H₅O₇) and the crystals diffracted well. The crystal structure of FN B-8 was determined by molecular replacement of previously solved FN-8 (RSCB code 1fnf). The structure was refined to 2.01 Å (Table 1) with R=24.9% and R_{free}=30.1% (Fig 1A–C). We were unable to completely trace the N-terminal histidine tag and several amino acids thereafter. This highly flexible N-terminal portion may contribute to slight increased of the R values. However, these refinement statistic values are mimicking the ones of the 2.0 Å of the crystal structure of type III fibronectin solved previously.⁴

FN B-8 appears to be a monomeric structure in one crystallographic asymmetric unit. Like other crystal structures in the fibronectin family, the overall structure of FN B-8 is composed of two copies of β sandwich globular domains (Fig 1B). Each β sandwich domain is formed by an intimate anti-parallel embrace of three anti-parallel β-strands (A, B, and E) on one side, and four anti-parallel β-strands (C', C, F, and G) on the opposite side.

The general framework of the EIIIB is almost identical to the NMR structure of FN-B (RSCB code: 2fnb; Fig 1D).²¹ However, the crystal structure showed clearly that the formation of longer anti-parallel β-strands compared to the NMR structure. The rmsd between the C_α positions of our crystal structure and the NMR structure is as close as 2.5 Å. This allows us to validate our phasing information since we did not use the NMR structure for our molecular replacement. We believe that the molecular arrangement and packing of the crystal may contribute tightly β strand to β strand relationship in our structure compared to the NMR one.

The overall fold of FN-8 is also similar to the previous crystal structure (rmsd =4.2 Å; Fig 1D). The only obvious change in our FN-8 structure is the formation of extra β-G' strand. While, this alteration is possibly caused by crystal packing, it is clear that the additional extra domain B has minimal effect on the overall structural arrangement of FN-8.

FN-B Structurally Alters Macromolecular Structure of Fibronectin

We further compared our EIIIB with the previously solved FN-7. As expected, the overall frameworks of EIIIB and FN-7 are also very similar (rmsd=3.3 Å). The only noticeable alteration in the structural framework is that the β-E strand of the EIIIB seems to be longer and more structured than the one of FN-7 (Fig. 2A). While the general architectures of the EIIIB and FN-7 are alike, the interactions between FN-7 and FN-8 are distinctively different from the ones of EIIIB and FN-8.

When we superimposed FN-8 of our structure and FN-8 of 1fnf structure, we discovered three distinctions between the FN-7/FN-8 and FN-B/FN-8 structures (Fig 2A). First, the bending angle between EIIIB and FN-8 in our structure appears to be approximately 63° or about 11° more than the angle between FN-7 and FN-8 (previously reported 52°).⁴ Secondly, the rotating angle between EIIIB and FN-8 is approximately 117° or about 5° different from the one between FN-7 and FN-8 (previously reported 112°).⁴ Finally and perhaps most importantly, the locations and conformations of AB, CC', and EF loops of FN-B are different from the ones of FN-7.

FN-B and FN-8 Interface

The location and conformation of EF loops are the most conserved among other loops in the interface. The more acute bending of AB loop in domain B allows the dimer to bend further, which coincides with the rotation of the domain B and the opening of CC' loop. The interdomain linker between EIIIB and FN-8 buries 416 Å² of surface area, while the interdomain linker between FN-7 and FN-8 buries 587 Å² of surface area. The insertion of EIIIB clearly opens up the buried surface over 170 Å². The buried interface of EIIIB and FN-8 (416 Å²) is also less than the one between FN-8 and FN-9 (527 Å²), but more than the one between FN-9 and FN-10 (333 Å²). Therefore, the interface of EIIIB and FN-8 is the second smallest buried interface among the known FN-III interdomain interfaces. The smallest FN-III buried interface belonging to FN-9 and FN-10 is believed to allow the RGD sequence of FN-10 and the synergy sequence (PHSRN) of FN-9 to function together in the interaction with integrin.^{4,7} This alteration in the buried interface and the size of the FN B-8 interface suggest that it is possible that the CC' loop between the interface of EIIIB and FN-8 may behave akin the RGD of FN-10 and the synergy region of FN-9.

We further examined the electrostatic potential surface of FN B-8 (Fig 2B). The CC' loop of EIIIB forms an acidic groove with FN-8. In addition, The AGEQIP sequence of the CC' loop of EIIIB is distinct from the NGQQGN sequence of the CC' loop of FN-7 (Fig 1A). An equivalent acidic groove, forming by the CC' loop and its adjacent domain, was also identified in another FN-III-like structure, the FN-III domains of the cytoplasmic tail of integrin β4.²² The sizes of these two homologous acidic grooves are almost the same, approximately 20 × 10 Å. The acidic groove and the CC' loop were proposed to be potential protein-protein interacting sites.²² We also found that the neighboring molecule in the crystal structure packs in nicely into this acidic groove. The opened CC' loop of EIIIB and the rotated and tilted of EIIIB domain allow a good access to the FG loop of FN-8, which is normally hindered by the CC' loop of FN-7 (Fig 2A).

Defining the Potential Protein Binding Site

We have determined the high resolution crystal structure of the FN type III domains EIIIB and 8 and compared it with the known structure of FN type III domains 7 & 8. Of interest was the buried interdomain interface between EIIIB and FN-8 and its comparison to the one of FN-7 and FN-8. Our crystal structure of FN B-8 shows that the interface between EIIIB and FN-8 is the second smallest of known FN-III structures and the CC' loop of EIIIB forms a unique acidic groove with the FN-8. The groove is large enough to allow the neighboring molecule in the crystal to pack. In addition, the bending angle between EIIIB and FN-8 in our structure appears to be tilted about 11° more than the angle between FN-7 and FN-8. The rotating angle between EIIIB and FN-8 is also approximately 5° different from the one between FN-7 and FN-8. Given the rotation angles between the various type-III domains of FN (7–10) and the biologic significance attached to it (e.g., RGD and PHSRN loops in domains 10 and 9 respectively), it was speculated that insertion of EIIIB between domain 7 & 8 could alter the downstream structure by causing the domains to be flipped. Our data suggest that insertion of EIIIB may not have any downstream effects with respect to alteration of domain polarity. Finally and perhaps most significantly, the locations and conformations of AB, CC', and EF loops of FN-B are different from the ones of FN-7.

Proposed Potential Protein Binding Site

Although the expression of spliced domain EIIIB is highly regulated during embryonic development, wound healing and tumorigenesis, there is no well defined function for this spliced domain of FN. Interestingly, even the EIIIB-null mice fail to reveal a clear function for domain EIIIB although embryonic fibroblasts prepared from the EIIIB^{-/-} mice showed slower

proliferation and the FN fibrils assembled by these embryonic fibroblasts were shorter and thinner compared to those deposited by the wild type fibroblasts.¹² These findings suggest that FN EIIIB may play a specific role in the regulation of particular matrix assembly and FN matrix-dependent cell growth. It has been shown that EIIIB-containing FN produced by cultured chondrocytes is preferentially incorporated in the cartilage matrix. EIIIB+ FN has also been described in the walls of smaller blood vessels, smooth muscle of the gastro-intestinal and respiratory tracts and cartilaginous structures.¹⁵

FN is known to utilize short-peptide surface loops in engaging its interactions with other proteins in the signaling pathway, for example the RDG sequence of FN-10,⁶ the PHSRN sequence of FN-9,²³ and the KNEED sequence of FN-8.²⁴ Based on our crystal structure, it is tempting to speculate that the AGE GIP sequence of CC' loop of EIIIB may be a potential site for protein binding. However, there is no evidence at present that the AGE GIP is the protein binding site and studies are in progress to further examine this potential binding site. Preliminary analysis of cell lysates showed several proteins (data not shown) binding to FN 7-EIIIB-8 and not FN 7-8 in a reproducible manner (affinity chromatography and 2D gel analysis three times). Further characterization of binding proteins to the FN 7-EIIIB-8 is in progress.

Protein Data Bank accession number

The structural coordinate was deposited to the Protein Data Bank (RCSB code: 2GEE).

Acknowledgements

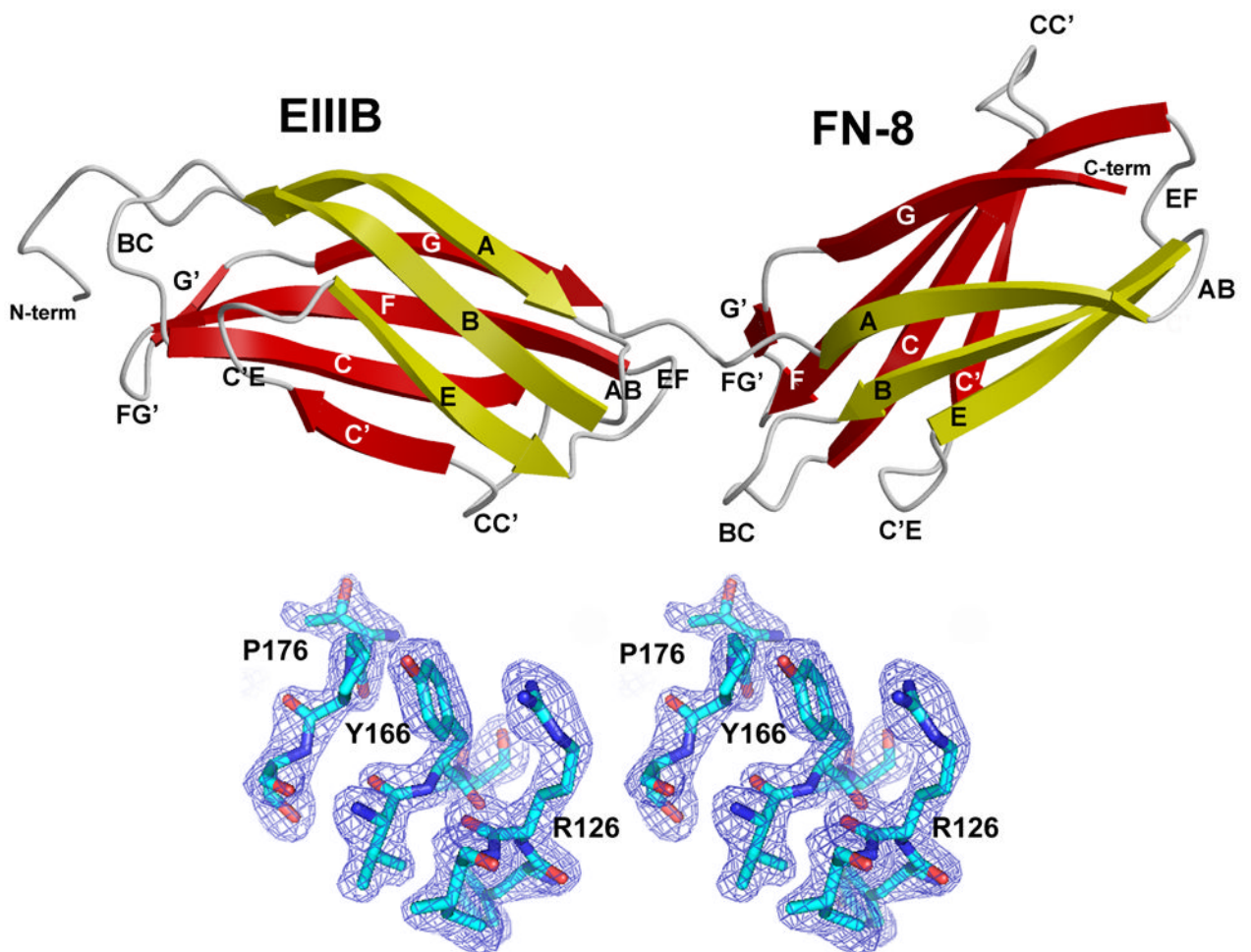
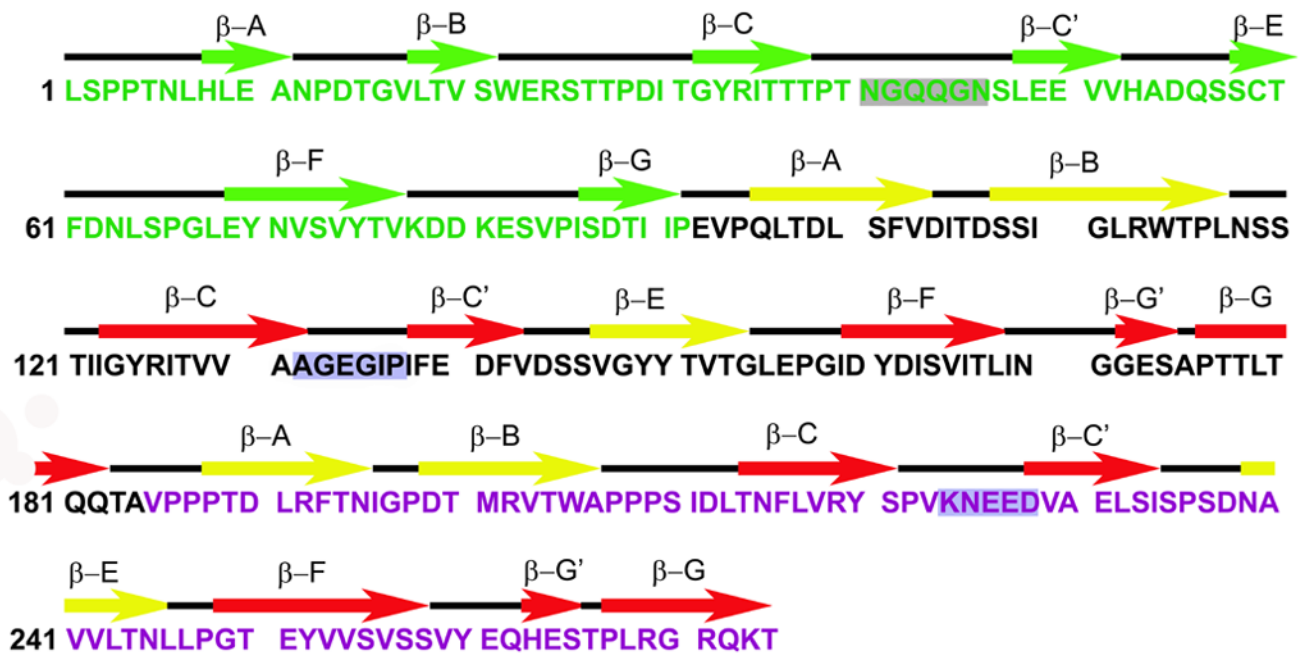
We thank Laurie Betts, Kent Rossman, and Brant Hamel for experimental assistance. The research was supported by the N.I.H. DE-014394 (I.A.), the University of North Carolina-Research Council Grant (S.B.), and the UNC-School of Dentistry-Faculty Creativity Fund (S.B.).

References

1. Hynes, RO. Fibronectins. New York: Springer Verlag; 1990.
2. George EL, Georges-Labouesse EN, Patel-King RS, Rayburn H, Hynes RO. Defects in mesoderm, neural tube and vascular development in mouse embryos lacking fibronectin. *Development (Camb)* 1993;119:1079–1091.
3. Kornblihtt AR, Vibe-Pedersen K, Baralle FE. Human fibronectin: cell specific alternative mRNA splicing generates polypeptide chains differing in the number of internal repeats. *Nucleic Acids Res* 1984;12:5853–5868. [PubMed: 6462919]
4. Leahy DJ, Aukhil I, Erickson HP. 2.0 Å crystal structure of a four-domain segment of human fibronectin encompassing the RGD loop and synergy region. *Cell* 1996;84:155–164. [PubMed: 8548820]
5. Pierschbacher MD, Ruoslahti E. Cell attachment activity of fibronectin can be duplicated by small synthetic fragments of the molecule. *Nature* 1984;309:30–33. [PubMed: 6325925]
6. Obara M, Kang MS, Yamada KM. Site-directed mutagenesis of the cell-binding domain of human fibronectin: separable, synergistic sites mediate adhesive function. *Cell* 1988;53:649–657. [PubMed: 3286012]
7. Takagi J, Strokovich K, Springer TA, Walz T. Structure of integrin alpha5beta1 in complex with fibronectin. *EMBO J* 2003;22:4607–4615. [PubMed: 12970173]
8. Hynes RO. Integrins: bidirectional, allosteric signaling machines. *Cell* 2002;110:673–687. [PubMed: 12297042]
9. Takagi J. Structural basis for ligand recognition by RGD (Arg-Gly-Asp)-dependent integrins. *Biochem Soc Trans* 2004;32:403–406. [PubMed: 15157147]
10. Hynes RO. The emergence of integrins: a personal and historical perspective. *Matrix Biol* 2005;23:333–340. [PubMed: 15533754]
11. Schwarzbauer JE, Patel RS, Fonda D, Hynes RO. Multiple sites of alternative splicing of the rat fibronectin gene transcript. *EMBO J* 1997;6:2573–258. [PubMed: 2445560]

12. Fukuda T, Yoshida N, Kataoka Y, Manabe R, Mizuno-Horikawa Y, Sato M, Kuriyama K, Yasui N, Sekiguchi K. Mice Lacking the EDB Segment of Fibronectin Develop Normally but Exhibit Reduced Cell Growth and Fibronectin Matrix Assembly in Vitro. *Cancer Res* 2002;62:5603–561. [PubMed: 12359774]
13. Astrof S, Crowley D, George EL, Fukuda T, Sekiguchi K, Hanahan D, Hynes RO. Direct Test of Potential Roles of EIIIA and EIIIB Alternatively Spliced Segments of Fibronectin in Physiological and Tumor Angiogenesis. *Mol Cell Biol* 2004;24:8662–8670. [PubMed: 15367684]
14. Ffrench-Constant C, Hynes RO. Alternative splicing of fibronectin is temporally and spatially regulated in the chicken embryo. *Development (Camb)* 1989;106:375–388.
15. Peters JH, Chen GE, Hynes RO. Fibronectin isoform distribution in the mouse. II. Differential distribution of the alternatively spliced EIIIB, EIIIA, and V segments in the adult mouse. *Cell Adhes Commun* 1996;4:127–148. [PubMed: 8937747]
16. Castellani P, Viale G, Dorcaratto A, Nicolo G, Kaczmarek J, Querze G, Zardi L. The fibronectin isoform containing the ED-B oncofetal domain: a marker of angiogenesis. *Int J Cancer* 1994;59:612–618. [PubMed: 7525495]
17. Kaczmarek J, Castellani P, Nicolo G, Spina B, Allemanni G, Zardi L. Distribution of oncofetal fibronectin isoforms in normal, hyperplastic and neoplastic human breast tissues. *Int J Cancer* 1994;59:11–6. [PubMed: 7927891]
18. Mandel U, Gaggero B, Reibel J, Therkildsen MH, Dabelsteen E, Clausen H. Oncofetal fibronectins in oral carcinomas: correlation of two different types. *APMIS* 1994;102:695–702. [PubMed: 7946273]
19. Engel J, Odermatt E, Engel A, Madri JA, Furthmayr H, Rohde H, Timpl R. Shapes, domain organizations and flexibility of laminin and fibronectin, two multifunctional proteins of the extracellular matrix. *J Mol Biol* 1981;150:97–120. [PubMed: 6795355]
20. Erickson HP, Carrell N, McDonagh J. Fibronectin molecule visualized in electron microscopy: a long, thin, flexible strand. *J Cell Biol* 1981;91:673–678. [PubMed: 7328116]
21. Fattorusso R, Pellecchia M, Viti F, Neri P, Neri D, Wuthrich K. NMR structure of the human oncofoetal fibronectin ED-B domain, a specific marker for angiogenesis. *Structure* 1999;7:381–390. [PubMed: 10196121]
22. De Pereda JM, Wiche G, Liddington RC. Crystal structure of a tandem pair of fibronectin type III domains from the cytoplasmic tail of integrin alpha6beta4. *EMBO J* 1999;18:4087–4095. [PubMed: 10428948]
23. Aota S, Nomizu M, Yamada KM. The short amino acid sequence Pro-His-Ser-Arg-Asn in human fibronectin enhances cell-adhesive function. *J Biol Chem* 1994;269:24756–24761. [PubMed: 7929152]
24. Wong JY, Weng Z, Moll S, Kim S, Brown CT. Identification and validation of a novel cell-recognition site (KNEED) on the 8th type III domain of fibronectin. *Biomaterials* 2002;23:3865–3870. [PubMed: 12164191]
25. Aukhil I, Joshi P, Yan Y, Erickson HP. Cell- and heparin-binding domains of the hexabrachion arm identified by tenascin expression proteins. *J Biol Chem* 1993;268:2542–2553. [PubMed: 7679097]
26. Otwinowski, Z.; Minor, W. Data collection and processing. Daresbury Laboratories; Warrington: 1993.
27. Navaza J. Implementation of molecular replacement in AmoRe. *Acta Crystallogr D* 2001;57:1367–1372. [PubMed: 11567147]
28. Brunger AT, Adams PD, Clore GM, DeLano WL, Gros P, Grosse-Kunstleve RW, Jiang JS, Kuszewski J, Nilges M, Pannu NS, Read RJ, Rice LM, Simonson T, Warren GL. Crystallography & NMR system: a new software suite for macromolecular structure determination. *Acta Crystallogr D* 1998;54:905–921. [PubMed: 9757107]
29. Jones TA, Zou JY, Cowan SW, Kjeldgaard M. Improved methods for building protein models in electron density maps and the location of errors in these models. *Acta Crystallogr A* 1991;47:110–119. [PubMed: 2025413]
30. Read RJ. Improved Fourier coefficients for maps using phases from partial structures with errors. *Acta Crystallogr A* 1986;42:140–149.

31. Kraulis PJ. MOLSCRIPT: a program to produce both detailed and schematic plots of protein structures. *J Appl Crystallogr* 1991;24:946–50.
32. Esnouf RM. Further additions to MolScript version 1. 4, including reading and contouring of electron-density maps. *Acta Crystallogr D* 1999;55:938–40. [PubMed: 10089341]
33. Merritt EA, Murphy MEP. Raster3D version 2. 0 –a program for photorealistic molecular graphics. *Acta Crystallogr D* 1991;50:869–73. [PubMed: 15299354]



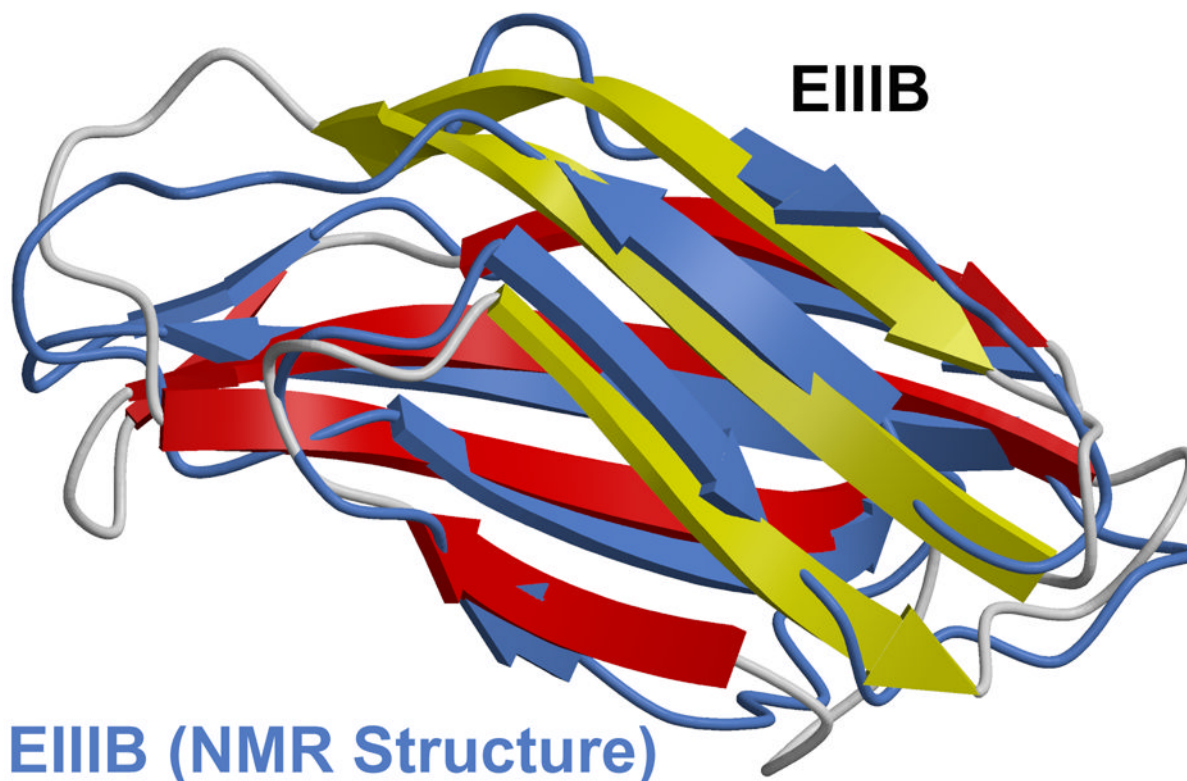


Figure 1. Crystal structure of FN-B8

(A) The primary and secondary structures of type III fibronectin domain 7, B and 8 are shown in green, black and magenta, respectively. The sequences of CC' loops of FN-7, FN-B and FN-8 are highlighted.

(B) A molscript diagram of FN B-8 structure. The β sandwiches are shown in yellow and red.

(C) 2.01 Å simulated annealing omit fofo electron density map contouring at 3.0σ . The map was calculated via $|F_{obs}| - |F_{calc}|$, ϕ_{calc} , with these amino acids and a sphere 1.0 Å around them omitted prior to annealing and map calculation. Part of β -C (residues 125–127), β -F (residues 165–167) and β -G (residues 175–177) strands of EIII-B are shown here.

(D) Superimposition of our EIII-B structure with previously solved NMR structure (RSCB code: 2fnb) demonstrates the similar overall folds.

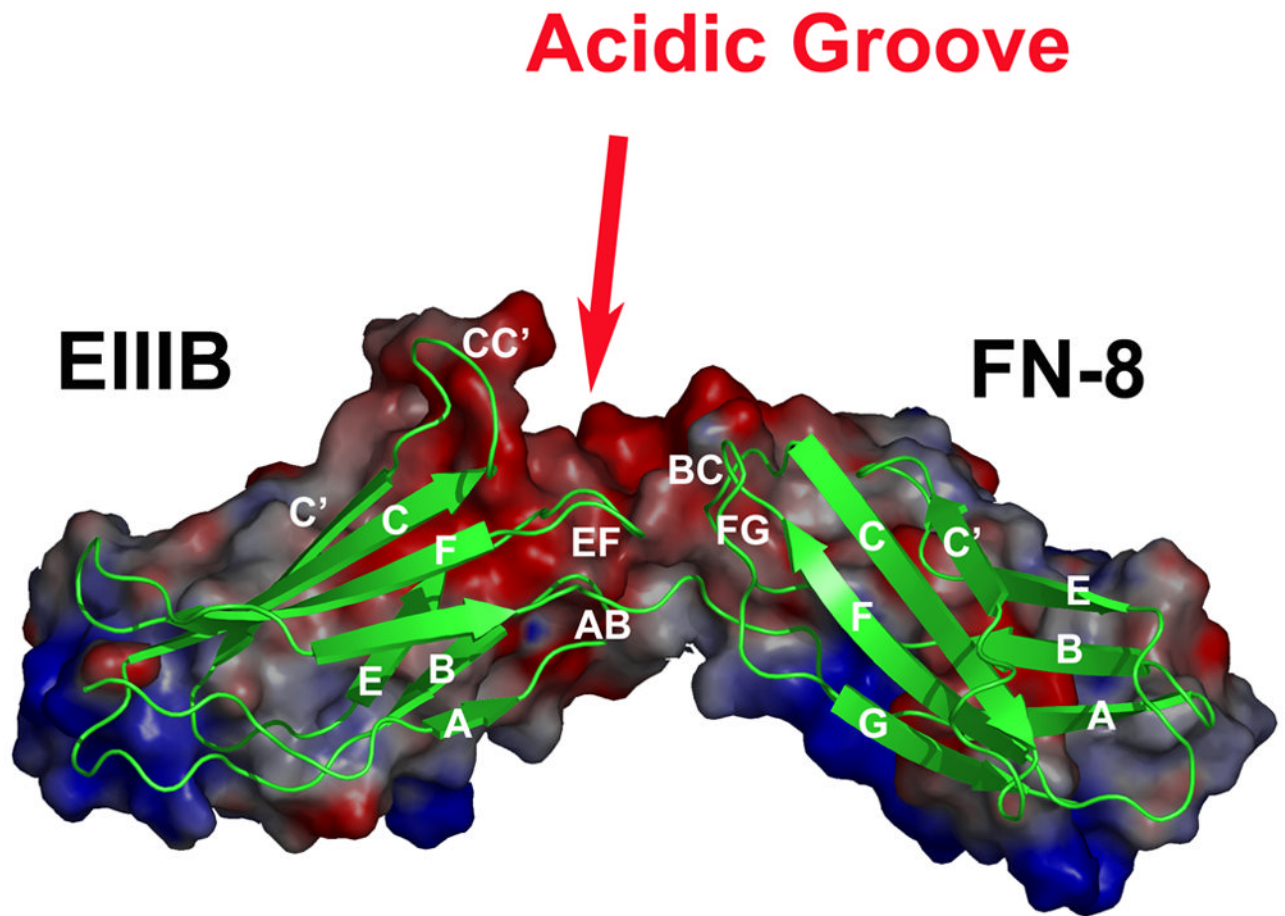


Figure 2. EIIIB alters the fibronectin structure

(A) Superimposition of EIIIB-8 of FN B-8 structure (shown in yellow/red) with FN 7-8 previously solved, RSBC code: 1fnf (shown in green), demonstrates that the differences in torsion and bending angles of FN B-8 compared with the FN 7-8; and the conformational differences of the AB, EF, and CC' loops in EIIIB and FN-7. The two orientations are related by a rotation of 180°.

(B) Molecular electrostatic potential surface representation of FN B-8 is colored by charge distribution (red negative, white neutral and blue positive) using program Pymol (DeLano, W.L., www.pymol.org).

Table 1

Protein expression and crystallization

A recombinant fragment of human – type III fibronectin FN-B and FN-8 (FN-B8) was amplified by PCR and subcloned into the pET15b expression vector. The protein was expressed and purified as previously described.^{4,25} FN-B8 was concentrated to 6 mg ml⁻¹ in 20 mM Tris pH 8.0, and crystallized using sitting drop vapor diffusion at 22°C. Crystals of 200–300 μm in size grew in 10% (w/v) PEG-3350 and 0.15–0.2 mM diammonium citrate ((NH₄)₂HC₆H₅O₇). The crystals were cryo-protected in 30–40% (v/v) glycerol plus 60–70% (v/v) mother liquor prior to flash cooling in liquid nitrogen.

Structure determination and refinement. Diffraction data were collected at the X-ray Facility at the University of North Carolina-Chapel Hill. The experiments were performed at 100 K using cryo-cooled crystals, and were processed and reduced using DENZO, SCALEPACK, and HKL2000.²⁶ The FN-B8 structure was determined by molecular replacement (AmoRe)²⁷ using the structure of FN-8 (RBSC code: 1fn1)⁴ as a search model. Residues 87–274 (188 residues) of the 223 amino acids were traced. Structures were refined using torsion angle dynamics in CNS²⁸ with the maximum likelihood function target, and included an overall anisotropic B-factor and a bulk solvent correction. About 10 percent of the observed data were set aside for cross-validation using free-R prior to any refinement. Manual adjustments were performed using the program O²⁹ and σ_A -weighted³⁰ electron density maps. Simulated annealing omit and σ_A -weighted difference density maps were used. Final structures exhibit good geometry with no Ramachandran outliers. Molecular graphic figures were created with MolScript,³¹ BobScript,³² Raster3D,³³ and Pymol (DeLano, W.L., www.pymol.org).

Resolution (Å; highest shell)	50-2.0 (2.13–2.01)
Space Group	P2 ₁ 2 ₁ 2 ₁
Cell Constants (Å, °)	a=43.41; b=55.29; c=74.90
Total Reflections	23182
Unique Reflections	12558
Mean Redundancy	6.2
R _{sym} ¹ (%; highest shell)	8.2 (48.3)
Completeness (%; highest shell)	99.6 (98.5)
Mean I/σ (highest shell)	36.6 (6.0)
R _{cryst} ² (%; highest shell)	24.9
R _{free} ³ (%; highest shell)	30.1
Number Protein Atoms	1443
Number Solvent Sites	384

¹R_{sym} = $\sum |I - \langle I \rangle| / \sum I$, where I is the observed intensity and $\langle I \rangle$ is the average intensity of multiple symmetry-related observations of that reflection.

²R_{cryst} = $\sum ||F_{obs}| - |F_{calc}|| / \sum |F_{obs}|$, where F_{obs} and F_{calc} are the observed and calculated structure factors, respectively.

³R_{free} = $\sum ||F_{obs}| - |F_{calc}|| / \sum |F_{obs}|$ for 10% of the data not used at any stage of structural refinement.